RSC Advances

PAPER

View Article Online
View Journal | View Issue

Cite this: *RSC Adv.*, 2025, **15**, 22534

Alginate integrated sodium ferrite nanocomposite-based dispersive solid-phase extraction for trace detection of metal ions in water and juices

Saima Perveen, [ab] Aysen Hol, [a] Jameel Ahmed Baig, *[b] Syed Tufail Hussain Sherazi, [b] Shahabuddin Memon, [b] Tasneem Gul Kazi, [b] Mohsin Kazi, [c] Khalid Hussain Thebo [d] and Khalil Akhtar [b]

In this work sodium ferrite nanoparticles ($Na_2Fe_4O_7$-NPs) were synthesized through a sol–gel green synthesis process using an aqueous extract of tamarind fruit and then combined with sodium alginate to synthesize composite AG/$Na_2Fe_4O_7$-NC. The synthesized nanoparticles and the composite were characterized by advanced analytical techniques to study crystalline behaviour, morphology, surface charge, and size distribution. AG/$Na_2Fe_4O_7$-NC was employed to develop a novel dispersive solid-phase extraction (DSPE) method for the simultaneous detection of heavy metals (HMs), including Cd, Co, Cu, Mn, Ni, and Pb, by flame atomic absorption spectrometry. Various experimental factors, including pH, nanocomposite dose, sample volume, eluent composition, eluent concentration, and eluent volume, were examined to maximize efficiency. The developed AG/$Na_2Fe_4O_7$-NC based DSPE method showed limits of detection (LODs) of 0.6, 0.2, 4.9, 1.0, 6.0, and 0.1 ng L^{-1} for Cd, Co, Cu, Mn, Ni, and Pb, respectively, with a preconcentration factor of 250. The accuracy of the method was validated using certified reference material (CRM), yielding excellent recovery rates between 97.1% and 98.7%. This developed method was successfully applied to measure HMs in tap water and fruit juice samples. The AG/$Na_2Fe_4O_7$-NC enhance the adsorption efficiency of the developed DSPE method and makes it a powerful tool for analyzing trace metals in environmental and food safety applications.

Received 19th March 2025
Accepted 24th June 2025

DOI: 10.1039/d5ra01948f

rsc.li/rsc-advances

1 Introduction

Environmental contamination is increasing daily due to several environmental contaminants, such as heavy metals (HMs), dyes, and pharmaceutical residues. Among them, the analysis of HMs is quite important for food safety, environmental protection, and the purity of materials. The investigation of HMs also holds importance in the field of agriculture to control environmental pollution. A lot of instrumental techniques for the quantitative measurement of HMs have been developed and employed. Flame atomic absorption spectrometry (FAAS) is widely applied for measuring HMs quantitatively as it is quite simple and cost-effective. The direct determination of HMs by FAAS is difficult due to their presence in trace quantities; therefore, the preconcentration step has been employed to measure the trace level of HMs in the environmental and food samples.[1]

Different methodologies, such as ion exchange,[2] electrochemical deposition,[3] liquid–liquid extraction (LLE),[4] cloud point extraction,[5] flotation,[6] dispersive solid phase extraction (DSPE),[7] and co-precipitation,[8] were applied for determining HMs. DSPE is superior in cost-effectiveness over other methods and is a good alternative to LLE.[9] The DSPE method is also preferred for preconcentrating HMs as it generates minimum solvent waste and reduces extraction time.[10] Moreover, the stable nature and wide surface area of the DSPE method result in efficient adsorption of HMs.[11] Many nanomaterials have been employed as sorbents for DSPE to enhance extraction efficiency. However, ferrite nanoparticles (FNPs) have shown maximum potential in efficiently removing HMs from environmental and food samples. This is due to their desirable features, *e.g.*, their large surface area and high chemical reactivity, resulting in efficient capture of HMs from the sample matrix.[12] FNPs have been synthesized using different synthesis methods, including hydrothermal, sol–gel, microwave, ultrasonic, precipitation, and chemical vapour deposition.[13] Moreover, the green synthesis of FNPs using the sol–gel method is of great importance as it is found cheaper and more eco-friendly method.[14,15] The green synthesis of FNPs uses extracts of biogenic species that contain biologically active compounds (amino acids, terpenoids, acetic acid, proteins, amides, ketones, aldehydes,

[a]*Chemistry Department, Pamukkale University, Denizli 20017, Turkey*
[b]*Centre of Excellence in Analytical Chemistry, University of Sindh, Jamshoro 76080, Pakistan. E-mail: jameel.baig@usindh.edu.pk*
[c]*Department of Pharmaceutics, College of Pharmacy, King Saud University, PO Box, 2457, Riyadh 11451, Kingdom of Saudi Arabia*
[d]*Institute of Metal Research Chinese Academy of Science, Shenyang, China*

and citric acid) essential for minimizing the aggregation of FNPs.[16] Tamarind (*Tamarindus indica*) is a well-known biogenic source due to its rich phytochemical composition, which includes citric acid, flavonoids, polyphenols, tartaric acid, and reducing sugars. These phytochemicals can effectively employed as reducing and capping agents in the green synthesis of FNPs. Furthermore, tamarind is cost-effective, abundantly available, and has previously demonstrated excellent performance in biogenic nanoparticle synthesis (*e.g.*, silver nanoparticles[17]), which makes it an efficient and sustainable selection for the synthesis of FNPs.[17,18] The FNPs possess a low adsorption capacity, resulting in a low recovery of HMs.[19] Thus, their properties can be improved by specific chemical modification *via* natural or synthetic polymers for the fabrication of their nanocomposite.[20] Natural polymers, mainly polysaccharides (for example, alginate), are preferable due to their structural porosity, hydrophilicity, ion-exchange ability, and active chemical functionalities of carboxyl and hydroxyl groups for binding HMs.[21]

The current study aims to synthesize sodium ferrite nanoparticles ($Na_2Fe_4O_7$-NPs) as the core material using a green method with tamarind fruit extract for the synthesis of an alginate-based core–shell composite (AG/$Na_2Fe_4O_7$-NC). The synthesized AG/$Na_2Fe_4O_7$-NC was applied to analyze HMs, including Cd, Co, Cu, Mn, Ni and Pb using the DSPE-based FAAS method. The $Na_2Fe_4O_7$-NPs and AG/$Na_2Fe_4O_7$-NC were thoroughly characterized by advanced analytical techniques to study crystalline structure, surface functionality, charge, morphology and particle size distribution. The AG/$Na_2Fe_4O_7$-NC was applied for the simultaneous determination of Cd, Co, Cu, Mn, Ni, and Pb in tap water and juice samples in trace quantities by dispersive solid-phase extraction (AG/$Na_2Fe_4O_7$-DSPE). The experimental factors were optimized to obtain excellent results. The AG/$Na_2Fe_4O_7$-DSPE was applied to determine traces of HMs in tap water and juice samples. The method allows for the detection of multiple metals in a single run, saving time and resources compared to methods that detect each element separately.

2 Experimental work

2.1 Standards and chemicals

Analytical-grade standards and chemicals were employed in all the experimental studies. The certified reference material (CRM; SPS Waste Water level 2), was obtained from the Spectrapure Standards (Oslo, Norway). The chlorides of nickel, sodium, calcium, manganese, cobalt, and chromium, the carbonates of calcium, the sulfate salt of magnesium, and the nitrates of sodium, potassium, and iron were purchased from Fluka (Bush, Switzerland). The sodium acetate (CH_3COONa), ammonium hydroxide (NH_4OH), hydrochloric acid (HCl), nitric acid (HNO_3), sulfuric acid (H_2SO_4), and the standard stock solutions of Cd, Co, Cu, Mn, Ni, and Pb of 1000 mg L^{-1} were also purchased from Sigma-Aldrich, Louis, USA. The distilled water was obtained from the ultra-pure water purifier system (Bedford, USA).

2.2 Instrumentation

A digital pH meter (Model pH 2700) with a glass electrode was purchased from Eutech, Malaysia. The Fourier transform infrared (FTIR) spectrophotometer of Nicolet (Madison, WI) and scanning electron microscopy (SEM) instrument of JEOL (JSM-7600F, Japan) were used to determine the functional groups and surface morphology of synthesized materials, respectively. An X-ray diffraction (XRD) instrument of Bruker (Wisconsin, USA) was used to study the crystalline structure of synthesized materials. The zeta potential (ZP) and zeta size (ZS) of synthesized materials were analyzed by a Dynamic Light Scattering system (ELSZ-2000). A FAAS instrument (PerkinElmer Analyst 200, Norwalk, CT, USA) was used for elemental analysis with a custom-built micro-sample injection system (MIS). A hollow-cathode lamp was employed for the measurement of Cd, Co, Cu, Mn, and Ni. The EDL lamp was employed for Pb measurement. The spectral line for Cd, Co, Cu, Mn, Ni, and Pb was selected as 228.8, 240.7, 324.8, 279.5, 232.0, and 217.0 nm, respectively. A Milestone (ETHOS EASY) microwave digestion device (Germany) was used to digest the juice samples.

2.3 Sol–gel green synthesis of $Na_2Fe_4O_7$-NPs

The tamarind fruit was purchased from the supermarket of Pamukkale-Denizli, Turkey, and washed with distilled water. Aqueous extract of tamarind fruit was prepared by taking ten grams of tamarind fruit in 200 mL of distilled water. The mixture was heated at a temperature of 70 °C on a hot plate for 120 minutes with continuous stirring. The prepared extract was filtered and used to synthesize $Na_2Fe_4O_7$-NPs.[22] After extraction preparation, 100 mL of iron nitrate nonahydrate (2.0 M) and sodium nitrate (1.0 M) were prepared separately and stirred to get clear solutions. Then the prepared solutions were mixed, and 200 mL of prepared extract was poured slowly with the help of a burette. The pH of the solution was maintained from 7.0–9.0 with NH_4OH. Then, the solution was stirred on a hot plate at 80 °C for two hours. After being dried in a hot air oven, the final product was pulverized with a pestle and mortar. The obtained powder was calcined at 850 °C for 5 hours for the phase development of $Na_2Fe_4O_7$-NPs.[23,24]

2.4 Synthesis of AG/$Na_2Fe_4O_7$-NC

AG/Na_2Fe_4O7-NC was synthesized using $Na_2Fe_4O_7$-NPs.[21] This composite was made by mixing 100 mL of a 3% (w/v) sodium alginate solution with 1 g of $Na_2Fe_4O_7$-NPs and stirring the mixture for three hours. After adding the combination dropwise to 100 mL of a 2% (w/v) $CaCl_2$ solution, it was left overnight. To get AG/$Na_2Fe_4O_7$-NC, the resultant material was filtered, completely cleaned with distilled water, dried for 24 hours at 30 °C, and crushed into a fine powder.

2.5 DSPE-FAAS procedure for the determination of HMs by AG/$Na_2Fe_4O_7$-NC

The DSPE procedure involved the mixing of 0.02 g of AG/$Na_2Fe_4O_7$-NC in 500 mL of a 20 μg L^{-1} solution of Cd, Co, Cu, Mn, Ni, and Pb. The suspensions of different pH ranges from

2.0–9.0 were prepared using buffer solutions. The prepared suspensions were vortexed thoroughly for 30 s. The samples were then divided into multiple 50 mL centrifuge tubes and centrifuged accordingly at 3000 rpm for 3 min. The supernatant was discarded, and 5 mL of eluent (HNO_3; 0.5 M) was mixed with the AG/$Na_2Fe_4O_7$-NC, which was loaded with HMs. This suspension was vortexed for 30 s and then centrifuged at 3000 rpm for 3 min. The resulting supernatant was separated and detected by FAAS for the determination of HMs.

2.6 Application of CRM and real samples

The devised technique was used to evaluate the known concentration CRM (SPS Waste Water level 2), and FAAS conducted triple analyses. Samples of tap water were gathered, filtered, and stored in Denizli, Turkey. The juice boxes of several brands were purchased from stores in Denizli, Turkey. The concentrated HNO_3 and H_2O_2 (5 : 1 by volume) were poured into 10 mL of the juice samples, followed by being subjected to microwave digestion.[25] The resulting product was diluted up to 500 mL with distilled water. The developed AG/$Na_2Fe_4O_7$-NC-based DSPE-FAAS was employed for quantifying HMs in tap water and juice samples.

3 Results and discussion

3.1 Characterization

The synthesized nanoferrites were characterized by XRD for investigation of structure, size and % crystallinity. The XRD spectra of $Na_2Fe_4O_7$-NPs and AG/$Na_2Fe_4O_7$-NC are given in Fig. 1(a). The diffraction peak patterns obtained from the XRD spectrum of $Na_2Fe_4O_7$-NPs confirmed the formation of a hexagonal crystallite phase.[26,27] Further, it the XRD spectrum of AG/$Na_2Fe_4O_7$-NC showed similarities in the diffraction peak patterns to $Na_2Fe_4O_7$-NPs, and some peaks also disappeared due to the coating of sodium alginate on the $Na_2Fe_4O_7$-NPs. No other peak relevant to biopolymer was found in the range of 20–80° which confirmed the successful synthesis of AG/$Na_2Fe_4O_7$-NC.[27,28] The sharpness of peaks displays a higher degree of crystallinity. The average crystallite size was calculated by Debye–Scherrer formula which was found 21.8 and 39.3 nm, respectively. The crystallinity (%) of $Na_2Fe_4O_7$-NPs and AG/$Na_2Fe_4O_7$-NC was found to be 86 and 79%, respectively.

The presence of functional groups in sodium alginate (AG), $Na_2Fe_4O_7$-NPs, and AG/$Na_2Fe_4O_7$-NC was investigated by FTIR spectroscopy as shown in Fig. 1(b).[29] The peaks (3249 and 1638 cm^{-1}) were observed in the FTIR spectrum of $Na_2Fe_4O_7$-

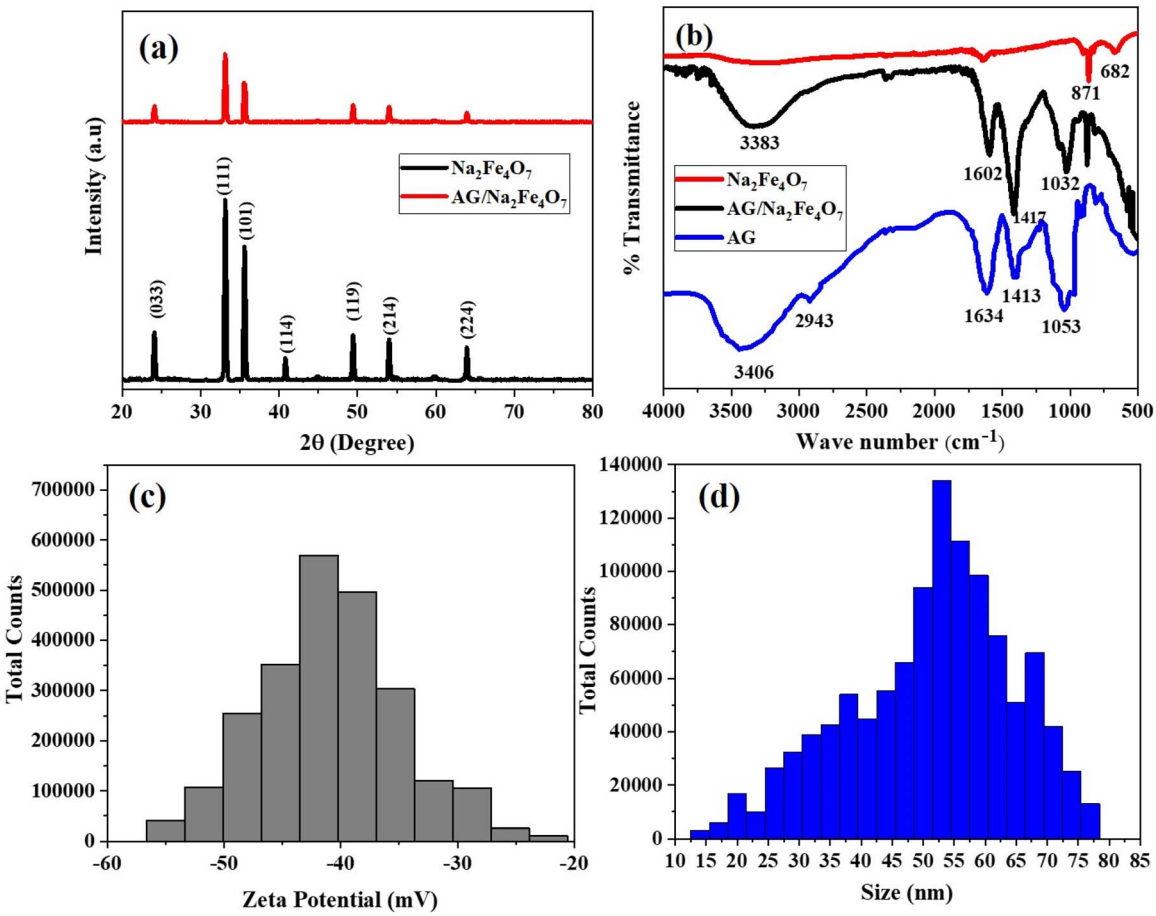

Fig. 1 (a) X-ray diffraction spectrum (b) Fourier transform infrared spectrum (c) zeta potential histogram and (d) zeta size histogram of AG/$Na_2Fe_4O_7$-NC.

NPs due to the stretching and bending of the hydroxyl group, resulting in moisture adsorption by $Na_2Fe_4O_7$-NPs.[30] Another, absorption peak was found at 682 cm^{-1} that was attributed iron–oxygen (Fe–O) stretching vibration. The peak at 871 cm^{-1} that was reported as distinct peak of hexagonal ferrites was also observed.[31] In the FTIR spectrum of AG the peak observed at 3406, and 2943 cm^{-1} are due to the stretching vibration of the hydroxyl, and methylene group of alginate, respectively.[32,33] The peaks observed at 1413 and 1634 cm^{-1} are due to symmetric and asymmetric C=O stretching vibrations of carboxyl group. The carbon–oxygen (C–O) stretching vibration was observed at 1053 cm^{-1}.[32,34–37] Moreover, in the FTIR spectrum of AG/$Na_2Fe_4O_7$-NC all the peaks of AG was observed with slight shifting and peak of Fe–O was also observed indicating successful formation of AG/$Na_2Fe_4O_7$-NC. The presence of hydroxyl and carboxyl acid groups in AG is responsible for the effective adsorption of HMs.

Further, the zeta potential is a critical parameter that reflects the stability of nanoparticles within a colloidal dispersion.[38] It measures the electrostatic potential at the interface of the double layer surrounding a colloidal particle in solution. Particles with zeta potentials between −10 mV and +10 mV are considered neutral, while those with potentials less than −30 mV or greater than +30 mV are categorized as strongly anionic or cationic, respectively.[39] The zeta potential of AG/$Na_2Fe_4O_7$-NC was investigated and found in the range of −22.2 mV to −54.9 mV, with an average value of −40.87 mV (Fig. 1(c)). This strongly anionic nature suggests excellent stability and enhances the material's ability to adsorb cationic heavy metals. Additionally, the zeta size (ZS) of AG/$Na_2Fe_4O_7$-NC was determined by plotting the size against total counts, which showed the size ranged from 14 to 77 nm, with an average size of 51.3 nm (Fig. 1(d)).

Moreover, SEM was used to investigate the surface morphology of synthesized $Na_2Fe_4O_7$-NPs and AG/$Na_2Fe_4O_7$-NC as shown in Fig. 2(a) and (b).[40,41] The SEM image of $Na_2Fe_4O_7$-NPs displayed a semi-spherical shape of agglomerated particles with porous and rough surfaces. The surface properties of $Na_2Fe_4O_7$-NPs can maximize the adsorption of HMs by possessing a large surface area.[42,43] From the SEM analysis AG/$Na_2Fe_4O_7$-NC it was observed that the shape of particles changed and size was also increased due to the covering of sodium alginate resulting in a highly rough surface. The increase in roughness of the surface further enhances the surface area of AG/$Na_2Fe_4O_7$-NC. Consequently, the synthesized nanocomposite can be proved effective for the adsorption of HMs.

The elemental composition of synthesized AG/$Na_2Fe_4O_7$-NC was investigated by EDX to confirm the formation of AG/$Na_2Fe_4O_7$-NC. The results are shown in Fig. 3(a), which reveals

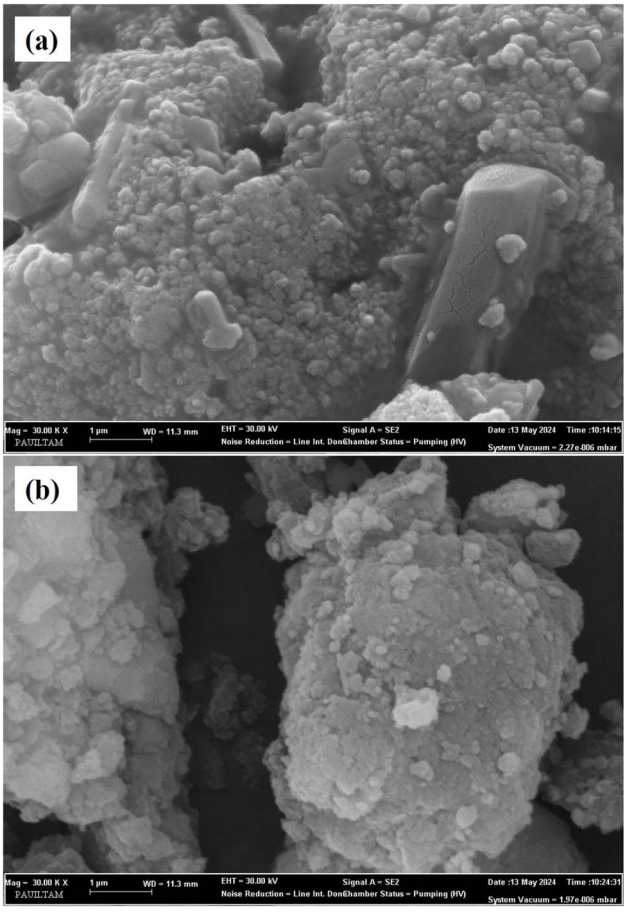

Fig. 2 SEM image of synthesized (a) $Na_2Fe_4O_7$-NPs and (b) AG/$Na_2Fe_4O_7$-NC.

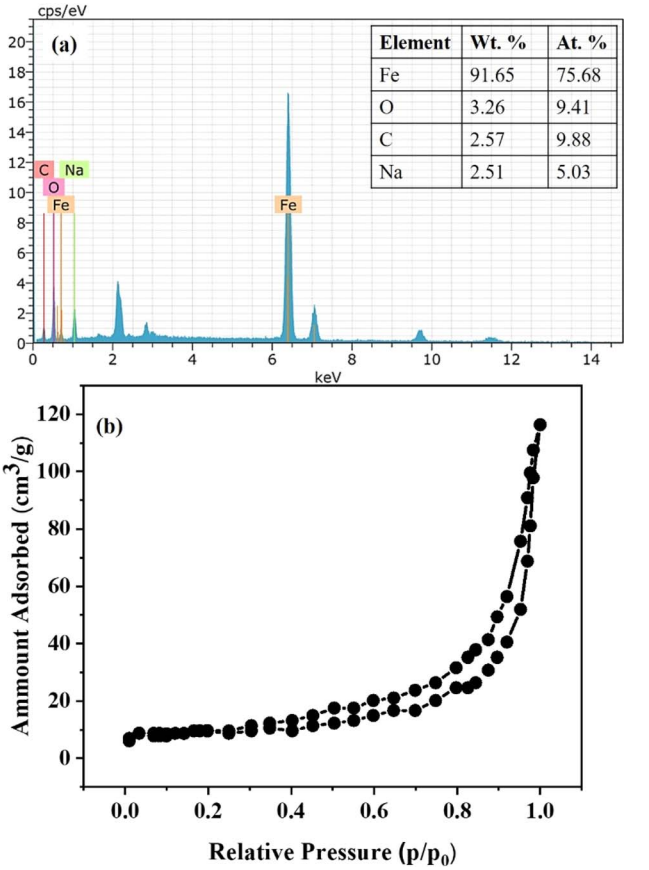

Fig. 3 (a) EDS and (b) BET of synthesized AG/$Na_2Fe_4O_7$-NC.

the presence of all desired elements (C, Na, O, and Fe) that confirm the successful synthesis of AG/$Na_2Fe_4O_7$-NC. Surface area and porosity of synthesized AG/$Na_2Fe_4O_7$-NC were analyzed by nitrogen adsorption desorption isotherm. The isotherm curve in Fig. 3(b) shows an IUPAC type IV isotherm with a type H3 hysteresis loop. According to the figure, the majority of the uptake takes place between relative pressures of 0.1 and 0.95. The AG/$Na_2Fe_4O_7$-NC exhibited a uniform pore width and the average pore size was found 18.387 AG/$Na_2Fe_4O_7$-NC. In addition, the average BET surface area was obtained 45.256 $m^2\ g^{-1}$ for AG/$Na_2Fe_4O_7$-NC which making AG/$Na_2Fe_4O_7$-NC best option for adsorption studies.

3.2 Optimization of DSPE factors

3.2.1 Influence of pH. The most crucial factor for the successful adsorption and retention of analytes (HMs) onto the adsorbent (AG/$Na_2Fe_4O_7$-NC) is the pH of the solution. As a result, the impact of pH was investigated throughout a broad pH range of 2–9, which was maintained using buffer solutions. According to obtained experimental results in Fig. 4(a), pH 6 was found suitable for detection of Cd, Co, Cu, Mn, and Ni as these HMs showed maximum recovery at this pH. However, it was observed that the maximum recoveries for Pb were found at pH 7. Nevertheless, there were no appreciable variations in Pb recoveries at pH 6 and 7. Therefore, pH 6 was selected as the optimal pH for the simultaneous determination of Cd, Co, Cu, Mn, Ni and Pb. The maximum recovery of HMs at pH 6 is further elucidated by considering the dissociation behavior of alginic acid and the chemistry of the HMs in solution. The pK_a value of alginic acid is approximately 3.5 which mean that almost 76% of the carboxyl groups are dissociated at pH 4, while more than 99% of dissociation of these groups occurs at pH 6 resulting in their deprotonation.[44] The dissociation of carboxyl groups increases the negatively charged carboxylate sites on the surface which enhances the chelation capacity of the AG/$Na_2Fe_4O_7$-NC. This improve the adsorption of positively charged HMs on the surface of AG/$Na_2Fe_4O_7$-NC.[45] However, further increase in pH showed decrease in recoveries of HMs leading to the formation of metal hydroxide species having lower solubility and tend to precipitate.[46] These precipitates can adhere to the walls of the container which effectively reduce the concentration of HMs available for adsorption onto the adsorbent surface.

3.2.2 Influence of adsorbent dose. In order to determine HMs using the established DSPE technique at pH 6, the impact

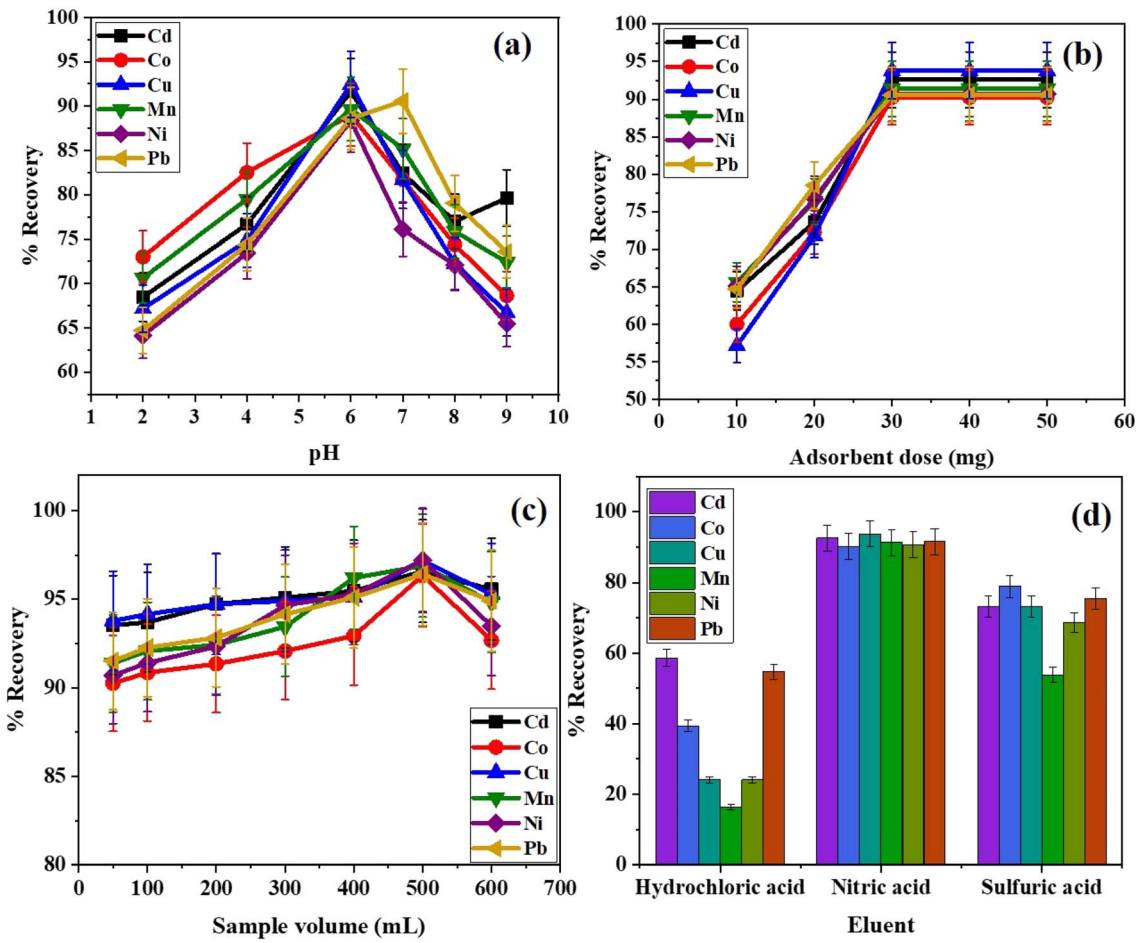

Fig. 4 Optimization of (a) pH, (b) adsorbent dose, (c) sample volume, and (d) eluent composition on the recoveries of Cd, Co, Cu, Mn, Ni, and Pb using AG/$Na_2Fe_4O_7$-NC based developed DSPE method.

of the adsorbent quantity was investigated between 10 and 50 mg (Fig. 4(b)). According to the results shown in Fig. 3(b), HM recoveries rose as the dose of AG/$Na_2Fe_4O_7$-NC increased by up to 30 mg. The HM recoveries nearly stay the same after 30 mg of AG/$Na_2Fe_4O_7$-NC, suggesting that there is an adequate dose of active site for HM adsorption at 30 mg of AG/$Na_2Fe_4O_7$-NC. Therefore, 30 mg of AG/$Na_2Fe_4O_7$-NC was utilized to determine the HMs.

3.2.3 Influence of sample volume. The influence of sample volume on the recovery of HMs was investigated by changing the volume from 50–600 mL while keeping experimental conditions constant. After preconcentration, the retained HMs were eluted using 2 mL of 1.0 M HNO_3 and quantified using FAAS (Fig. 4(c)). The results showed that the recovery of HMs increased with increasing sample volume up to 500 mL and then decreased after further increasing the sample volume. From the results, it was noted that at lower sample volumes, the number of HMs present may be insufficient to consume the capacity of the adsorbent completely and resulting in low recovery. By increasing the sample volume, more HMs are available to interact with the abundant carboxyl functional groups on the AG/$Na_2Fe_4O_7$-NC surface, which improves the recoveries of HMs. However, a further increase in sample volume beyond 500 mL leads to the saturation of the adsorbent, and the number of available active sites becomes insufficient to bind all HMs in the solution. This leads to lower recovery at higher sample volumes. Therefore, 500 mL was selected as the optimal sample volume, which offers the best cooperation between analyte availability and adsorbent capacity.

3.2.4 Selection of best eluent. Various acids such as HNO_3, HCl, and H_2SO_4 were studied as potential eluents for the elution of HMs, and the results are shown in Fig. 4(d). It was observed that the HNO_3 resulted in the highest recovery of HMs due to its strong oxidizing nature and ability to efficiently break the interaction between HMs and adsorbent. Therefore, HNO_3 was selected as the optimal eluent for further use. Subsequently, the concentration of the selected eluent was investigated, ranging from 0.1–1.5 M, and the results are shown in Fig. 5(a). It was noted that the recoveries of HMs increased with increasing concentration of eluent up to 1.0 M. Beyond this concentration, no significant increase was observed which is possibly due to saturation of desorption efficiency or matrix effects. Thus, the optimal concentration of 1.0 M of eluent was selected. Further, the eluent volume was optimized in the range of 2.0–20 mL and the results are shown in Fig. 5(b). It was found that the 2.0 mL showed maximum recoveries due to sufficient desorption of retained HMs with minimal dilution. Therefore, 2 mL of 1.0 M HNO_3 was selected as optimal eluent. Based on the optimized sample volume of 500 mL and eluent volume of 2.0 mL, the preconcentration factor (PF), defined as the ratio of sample volume to eluent volume, was calculated as 250.[47]

3.2.5 Interference and reusability. The interfering species may significantly influence the recoveries of Cd, Cu, Co, Mn, Ni and Pb by interacting with HMs or the surface of the adsorbent.[48] The effectiveness of the AG/$Na_2Fe_4O_7$-NC/DSPE/FAAS method was examined by analyzing the recoveries of HMs (20 μg L^{-1}) in the presence of different concentrations of interfering species including Na^+, K^+, Ca^{2+}, Mg^{2+}, Cr^{3+}, SO_4^{2-}, Cl^-, CH_3COO^-, CO_3^{2-}, NO_3^-, citric acid, tartaric acid, malic acid, glucose, fructose and sucrose. The results shown in Table 1 indicated that the foreign species have no significant influence on the recoveries of Cd, Cu, Co, Mn, Ni and Pb. This confirmed the accuracy and efficiency of the developed AG/$Na_2Fe_4O_7$-NC/DSPE/FAAS method for the analysis of HMs in real samples.

Further, the reusability of the synthesized AG/$Na_2Fe_4O_7$-NC was assessed over five consecutive cycles using the same procedure. The AG/$Na_2Fe_4O_7$-NC retained its adsorption efficiency with no significant loss in recoveries of HMs, which indicates the excellent chemical/mechanical stability and reusability of synthesized AG/$Na_2Fe_4O_7$-NC. This demonstrates that AG/$Na_2Fe_4O_7$-NC can be effectively reused at least five times with negligible decline in performance. Furthermore, the functional groups responsible for HMs binding remained intact, which was confirmed by consistent performance and minimal leaching during desorption. These outcomes validate that the AG/$Na_2Fe_4O_7$-NC is chemically robust and mechanically

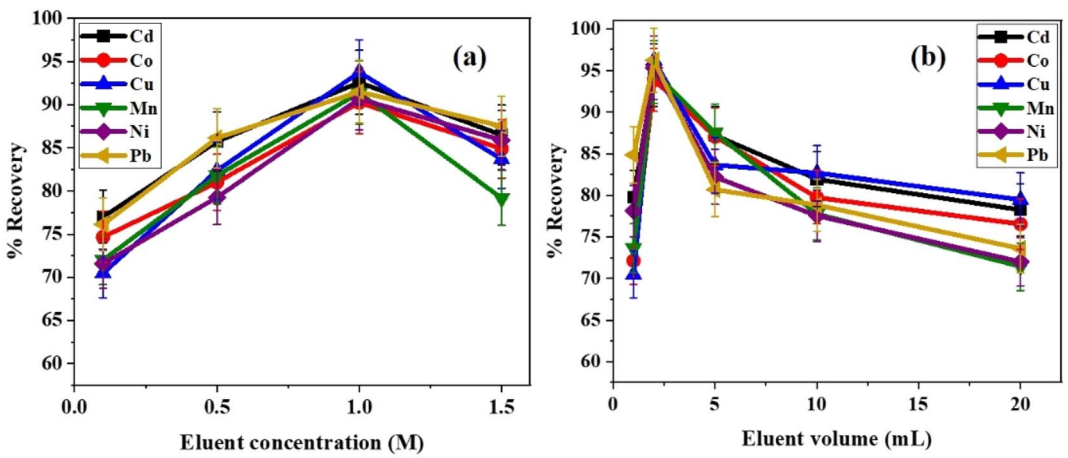

Fig. 5 Optimization of (a) eluent concentration and (b) eluent volume on the recoveries of Cd, Co, Cu, Mn, Ni, and Pb using AG/$Na_2Fe_4O_7$-NC based developed DSPE method.

Table 1 Influence of foreign species for the determination of HMs by AG/$Na_2Fe_4O_7$-NC-based SPE-FAAS method

Foreign species	Added salts	Tolerance limit (μg L^{-1})	% Recovery					
			Cd	Co	Cu	Mn	Ni	Pb
Na^+	NaCl	2000	93.4	92.3	94.4	95.1	92.2	93.7
K^+	KNO_3	100	94.2	92.1	96.4	93.4	91.6	94.2
Ca^{2+}	$CaCO_3$	1000	95.6	95.5	95.3	92.3	93.3	93.7
Mg^{2+}	$MgSO_4$	2000	95.1	94.3	94.1	96.1	96.6	94.6
Cr^{3+}	$CrCl_3$	100	94.6	96.6	96.4	96.4	94.2	95.4
SO_4^{2-}	$MgSO_4$	2000	92.3	91.8	95.8	95.3	93.4	94.4
Cl^-	NaCl	2000	93.5	93.3	95.7	95.3	96.5	95.6
CH_3COO^-	CH_3COONa	1000	94.3	96.3	93.5	93.7	95.8	96.5
CO_3^{2-}	$CaCO_3$	1000	91.5	94.5	93.2	94.2	93.9	92.8
NO_3^-	KNO_3	100	93.2	94.2	95.2	92.8	90.9	91.8
Citric acid	$C_6H_8O_7$	500	92.5	91.5	92.7	91.4	92.5	92.5
Tartaric acid	$C_4H_6O_6$	500	93.1	92.3	93.5	91.3	91.1	93.1
Malic acid	$C_4H_6O_5$	500	92.3	91.4	92.8	92.6	92.3	91.3
Glucose	$C_6H_{12}O_6$	1000	91.8	92.6	91.9	91.8	91.3	91.1
Fructose	$C_6H_{12}O_6$	1000	91.9	92.9	91.4	91.7	92.4	90.9
Sucrose	$C_{12}H_{22}O_{11}$	1000	91.4	92.5	91.5	91.6	91.8	90.4

durable, which makes it a reliable adsorbent for repeated application in DSPE.

3.2.6 Analytical figures of merit, validation, and application. The developed AG/$Na_2Fe_4O_7$-NC-based DSPE method's analytical figures of merit were carefully assessed. A number of variables, including concentration range, enrichment factor (EF), slope, intercept, correlation coefficient (R^2), limits of detection (LOD, S/N = 3.0), and limits of quantification (LOQ, S/N = 10) were investigated under ideal circumstances in order to assess the efficacy of the developed methodology.[49] The LODs and LOQs were calculated by using $3\sigma/s$ and $10\sigma/s$ formulas, respectively, where, σ is the standard deviation of blank (n = 10), and s is the slope of the calibration graph.[50] The LODs of the developed AG/$Na_2Fe_4O_7$-NC-based DSPE-FAAS method were found to be 0.0026, 0.0013, 0.0024, 0.0063, 0.0023, and 0.0023 μg L^{-1} for Cd, Co, Cu, Mn, Ni, and Pb, respectively. The EF was calculated by dividing the slope of the calibration curve with DSPE by the slope of calibration curve without DSPE.[51,52] The obtained EF values Cd, Co, Cu, Mn, Ni, and Pb were 249.3, 247.9, 247.6, 249.8, 248.9, and 248.8 which were approximately equal to that of PF. The findings show that trace levels of HMs in actual samples may be effectively analyzed concurrently using the new AG/$Na_2Fe_4O_7$-NC-based DSPE technique (Table 2).

The CRM was examined to evaluate the practical application of the AG/$Na_2Fe_4O_7$-NC-based DSPE method. The usefulness of the developed AG/$Na_2Fe_4O_7$-NC-based DSPE was studied and

Table 2 Analytical features of AG/$Na_2Fe_4O_7$-NC-based DSPE-FAAS method for the determination of HMs[a]

Without DSPE						
Parameter	Cd	Co	Cu	Mn	Ni	Pb
Dynamic range (μg L^{-1})	200–10 000	400–20 000	200–20 000	200–1000	200–20 000	400–20 000
Slope	0.02	0.0201	0.0104	0.0094	0.0222	0.0243
Intercept	0.0273	0.0287	0.0091	0.065	0.0284	0.0125
R^2	0.998	0.9992	0.9993	0.994	0.9998	0.997
LOD (μg L^{-1})	0.650	0.326	0.620	0.691	0.592	0.560
LOQ (μg L^{-1})	2.16	1.08	2.08	2.31	1.97	1.89
DSPE by AG/$Na_2Fe_4O_7$-NC						
Parameters	Cd	Co	Cu	Mn	Ni	Pb
Dynamic range (μg L^{-1})	2.00–80.0	4.00–80	2.00–80.0	2.00–80.0	2.00–80.0	4.00–80.0
Slope	4.986	4.9837	2.5752	2.348	5.5269	6.0468
Intercept	0.0283	0.0285	0.0063	0.09	0.0336	0.0108
R^2	0.998	0.9982	0.9998	0.999	0.9974	0.999
LOD (μg L^{-1})	0.0026	0.0013	0.0025	0.0063	0.0023	0.0023
LOQ (μg L^{-1})	0.0086	0.004	0.0084	0.009	0.0079	0.0076

[a] Note: LOD (limit of detection); R^2 (coefficient of determination); LOQ (limit of quantification).

Table 3 Application of AG/$Na_2Fe_4O_7$-NC based DSPE-FAAS methodology by quantitative determination of HMs by CRM

Heavy metal	Certified conc. (mg L^{-1})	Detected conc. (mg L^{-1})	Recovery (%)	RSD (%)
Cadmium	0.100 ± 0.0005	0.0982 ± 0.002	96.7–99.7	2.03
Cobalt	0.300 ± 0.002	0.293 ± 0.003	97.3–98.0	1.02
Copper	2.00 ± 0.01	1.942 ± 0.03	96.1–98.1	1.54
Manganese	2.00 ± 0.01	1.958 ± 0.04	96.4–99.4	2.04
Nickel	5.00 ± 0.0025	4.87 ± 0.10	95.4–99.4	2.05
Lead	2.00 ± 0.001	1.95 ± 0.03	93.6–98.1	1.54

Table 4 Application of the developed AG/$Na_2Fe_4O_7$-NC-based DSPE-FAAS methodology for the determination of HMs (μg L^{-1}) in tap water and juice samples

Samples	Pb	Cu	Co	Ni	Mn	Cd
Tap water	8.71 ± 1.3	4.64 ± 1.1	1.82 ± 0.3	2.39 ± 0.51	14.6 ± 2.5	0.75 ± 0.10
Apple	47.5 ± 6.1	21.63 ± 2.3	1.03 ± 0.1	9.53 ± 2.1	7.18 ± 1.9	12.8 ± 1.04
Orange	32.3 ± 3.7	32.60 ± 3.8	1.20 ± 0.1	19.61 ± 0.0	8.9 ± 1.25	19.1 ± 3.70
Apricot	26.8 ± 4.8	69.30 ± 4.7	5.17 ± 0.8	16.2 ± 1.09	48.7 ± 3.1	0.600 ± 0.01

recoveries of HMs were calculated. The resulting data of CRM samples indicated that the recoveries of HMs were found in the range of 93.62–99.70%, signifying the outstanding accuracy of the developed AG/$Na_2Fe_4O_7$-NC based DSPE method for the determination of HMs (Table 3).

The tap water samples ($n = 3$) were collected from Denizli, Turkey, filtered and stored. Fruit juices ($n = 9$) samples of different brands and flavors were collected from local markets in Denizli, Turkey. The juice samples include apples, oranges, and apricots. The juice samples were digested as mentioned above (in Section 2.5). The DSPE method was employed for the determination of HMs in tap water and juice samples. The results for tap water and juice samples are given in Table 4.

According to the results, Orange juices have the greatest content of Cd among the various fruit juices, followed by apple and apricot juices. Similarly, Apricot juices have the greatest concentrations of Cu, Co, and Mn, followed by orange and apple juice. Further, orange juices have the greatest Ni contents, followed by apricot and apple juice. Apple juices have the greatest concentration of Pb, followed by orange juice, while apricot juice has the lowest.

3.2.7 Estimated daily intake. Using the formula EDI = (CJ + CW)/BW, where CJ and CW represent the concentrations of HMs in a 200 mL juice pack and water, respectively, the estimated daily intake (EDI) of HMs was determined. For children and adults, the average body weight was 20 kg and 60 kg, respectively. The concentrations of HMs in Table 5 are below the FAO/WHO-determined provisional tolerated daily intake (PTDI).[53] A water contribution is also included in the HMs calculation. For instance, the daily water consumption of adults (2.5 L/age 20–25 years) and children (1.5 L/age 4–10 years) differs. The WHO recommended value is higher than the Turkish Food Codex, which is 0.1 mg L^{-1}. Accordingly, the provisional tolerable daily intake (PTDI) of HMs collectively through a regular juice pack per day and drinking water (tap water) consumed by children and adults is between 0.161 and 1.311 and 0.0673 to 0.680 μg kg per body weight per day, respectively.

3.2.8 Comparative study. The developed AG/$Na_2Fe_4O_7$-NC/DSPE/FAAS method has demonstrated more reliability than the already reported methods for the detection and quantification of HMs.[56–64] The novel adsorbent (AG/$Na_2Fe_4O_7$-NC) offers high extraction efficiency, a low LOD, and a high PF

Table 5 Calculated estimated daily intake and compared with PTDI level (3.57 μg kg per body weight per day)[54,55]

Metals	Concentration of metals in selected juice[a]	Juices consumed	Concentration of metals in tap water	Water consumed		Water and juice μg per L per day per body weight		FAO/WHO PTDI: μg per L per body weight per day	
				Children (1L)	Adults (3L)	Children	Adults	Children	Adults
Cd	10.8	2.16	0.750	0.750	2.25	0.16	0.067	0.357	1.00
Co	2.50	0.490	1.82	1.82	5.46	0.16	0.080	100	500
Cu	41.1	8.20	4.64	4.64	13.92	0.750	0.330	0.5	500
Mn	21.5	4.30	14.6	14.6	43.8	1.31	0.680	0.357	140
Ni	15.1	3.00	2.39	2.39	7.17	0.330	0.150	2.8	5.00
Pb	35.5	7.10	8.71	8.71	26.13	1.01	0.480	25.8	13.35

[a] The average concentration of HMs in selected juice samples.

Table 6 Comparison of the developed AG/$Na_2Fe_4O_7$-NC-based DSPE method with reported studies for the quantitative determination of HMs[a]

Method	Sorbent	Sorbent dose (mg)	Detection technique	PF	LOD (μg L^{-1})	Reference
mSPE	Luffa@TiO_2	5.00	FAAS	50.0	0.13	56
SPM	Bi_2WO_6	35.0	FAAS	50.0	6.0	57
DSP-Me	ND@Bi_2MoO_6	5.00	FAAS	24.5	1.75	58
Mspe	MWCNTs@$MgAl_2O_4$@TiO_2	5.00	FAAS	100	0.42	59
SPME	Nanodiamonds@NiCoFe-LDH	5.00	FAAS	25.0	0.621	60
MSPE	Alginate/MIL-101(Cr)-NH_2/Fe_3O_4	7.40	UHPLC-MS/MS	9.60	0.00043–0.0159	61
Batch flow	Fe_3O_4@MBA nano-hybrid	1000	AAS	—	—	62
Batch	Alg-Fe_3O_4	0.150	—	—	—	63
MSPE	Fe-alg-MgO	—	HPLC	—	0.0082–0.0139	64
DSPE	AG/$Na_2Fe_4O_7$	20.0	FAAS	250	0.0013–0.0063	Current study

[a] Note: FAAS; flame atomic absorption spectroscopy, mSPE; magnetic solid phase extraction, SPME; solid phase microextraction, DSPE; dispersive solid phase extraction, Fe_3O_4@MBA nano-hybrid; magnetite Fe_3O_4@biosilica/alginate, MSPE; magnetic solid phase extraction, Fe-alg-MgO; iron alginate magnetic graphene oxide, Alg-Fe_3O_4; sodium alginate-coated magnetite.

(Table 6). The results showed the outstanding performance of the AG/$Na_2Fe_4O_7$-NC/DSPE/FAAS method in terms of efficiency, sensitivity, and reliability for the analysis of HMs.

4 Conclusion

This study presented a green synthesis method for producing $Na_2Fe_4O_7$ nanoparticles ($Na_2Fe_4O_7$-NPs) using tamarind fruit extract, which was then used to create AG/$Na_2Fe_4O_7$-NC. The resulting AG/$Na_2Fe_4O_7$-NC exhibited nanoscale dimensions with a rough surface and high stability. A new dispersive solid-phase extraction flame atomic absorption spectrometry (DSPE-FAAS) method based on AG/$Na_2Fe_4O_7$-NC was developed for trace-level detection of heavy metals (HMs). The LODs of the developed method were found 0.0026, 0.0013, 0.0025, 0.0063, 0.0023, and 0.0023 μg L^{-1} for Cd, Co, Cu, Mn, Ni, and Pb, respectively. This DSPE-FAAS method was successfully applied to determine HMs in real water and juice samples. The estimated daily intake of HMs from the analyzed juice and water samples was also calculated and found to be below the provisional tolerable daily intake (PTDI) set by the WHO. Additionally, due to its simplicity and low LOD, this approach offers a superior alternative for the simultaneous determination of HMs compared to less effective and time-consuming methods.

Ethical statement

The current experimental investigations do not contain any kind of involvement, either direct or indirect of human contributors and animals.

Data availability

Access to the information that supports the current study will be provided at the official request.

Authour contributions

The current study owes its conceptualization, supervision, project administration, and review/editing to the esteemed efforts of Prof. Dr Aysen Hol along with Dr Jameel Ahmed Baig, Prof. Dr Syed Tufail Hussain Sherazi, Prof. Dr Shahabuddin Memon and Prof. Dr Tasneem Gul Kazi. Ms Saima Perveen, a dedicated PhD scholar, played a pivotal role in data curation, formal analysis, methodology, and creating the original draft. The technical aspects, including software usage, investigation, and visualization, were skillfully handled by Mohsin Kazi, Khalid Hussain Thebo, and Khalil Akhtar.

Conflicts of interest

All of the authors stated that they had no known financial or personal conflicts of interest that would have influenced research studies.

Acknowledgements

Thanks to the Chemistry Department, Pamukkale University, Denizli, Turkey, for support in current experimental activities. Their funding has been influential in the success of the present study and has passed the way for more discovery and exploration. The author would like to extend their sincere appreciation to the Ongoing Research Funding Program (ORF-2025-301), King Saud University, Riyadh, Saudi Arabia for the successful completion of this research study.

References

1 C. Duran, *et al.*, Solid-phase extraction of Mn(II), Co(II), Ni(II), Cu(II), Cd(II) and Pb(II) ions from environmental samples by flame atomic absorption spectrometry (FAAS), *J. Hazard. Mater.*, 2007, **146**(1–2), 347–355.
2 Z.-T. Jiang, J. C. Yu and H.-Y. Liu, Simultaneous determination of cobalt, copper and zinc by energy dispersive X-ray fluorescence spectrometry after preconcentration on PAR-loaded ion-exchange resin, *Anal. Sci.*, 2005, **21**(7), 851–854.
3 H. Matusiewicz and M. Lesiński, Electrodeposition sample introduction for ultra trace determinations of platinum group elements (Pt, Pd, Rh, Ru) in road dust by

electrothermal atomic absorption spectrometry, *Int. J. Environ. Anal. Chem.*, 2002, **82**(4), 207–223.

4 J. Wang, *et al.*, Investigation of the remaining major and trace elements in clean coal generated by organic solvent extraction, *Fuel*, 2005, **84**(12–13), 1487–1493.

5 M. A. Farajzadeh and M. R. Fallahi, Simultaneous cloud-point extraction of nine cations from water samples and their determination by flame atomic absorption spectrometry, *Anal. Sci.*, 2006, **22**(4), 635–639.

6 M. Hiraide, T. Ito, M. Baba, H. Kawaguchi and A. Mizuike, Multielement preconcentration of trace heavy metals in water by coprecipitation and flotation with indium hydroxide for inductively coupled plasma-atomic emission spectrometry, *Anal. Chem.*, 1980, **52**(6), 804–807.

7 G. P. Chandra Rao, S. S. Veni, K. Pratap, Y. Koteswara Rao and K. Seshaiah, Solid Phase Extraction of Trace Metals in Seawater Using Morpholine Dithiocarbamate-Loaded Amberlite XAD-4 and Determination by ICP-AES, *Anal. Lett.*, 2006, **39**(5), 1009–1021.

8 M. Soylak and N. D. Erdogan, Copper (II)–rubeanic acid coprecipitation system for separation–preconcentration of trace metal ions in environmental samples for their flame atomic absorption spectrometric determinations, *J. Hazard. Mater.*, 2006, **137**(2), 1035–1041.

9 M. Leon-Gonzalez and L. V. Perez-Arribass, Chemically modified polymeric sorbents for sample preconcentration, *ChemInform*, 2000, **902**(1), 3–16.

10 Z. Fan, B. Hu and Z. Jiang, Speciation analysis of vanadium in natural water samples by electrothermal vaporization inductively coupled plasma optical emission spectrometry after separation/preconcentration with thenoyltrifluoroacetone immobilized on microcrystalline naphthalene, *Spectrochim. Acta, Part B*, 2005, **60**(1), 65–71.

11 M. Hua, S. Zhang, B. Pan, W. Zhang, L. Lv and Q. Zhang, Heavy metal removal from water/wastewater by nanosized metal oxides: a review, *J. Hazard. Mater.*, 2012, **211**, 317–331.

12 Y. Zohrabi, Synthesis and application of magnetic ferrites (MFe_2O_4) in the removal of heavy metals from aqueous solutions: an updated review, *Mater. Sci. Eng., B*, 2024, **299**, 117024.

13 A. A. Oyekanmi, M. M. Hanafiah, T. T. Dele-Afolabi, A. Ahmad and M. B. Alshammari, Development of nanoparticles loaded composites from agricultural wastes for cationic dye removal from aqueous solution–a review, *J. Environ. Chem. Eng.*, 2022, **10**(5), 108263.

14 S. R. da Silva Ferreira, A. O. da Silva, J. A. L. Matias, A. R. Albuquerque, J. B. L. de Oliveira and M. A. Morales, Cashew gum as a sol-gel precursor for green synthesis of nanostructured Ni and Co ferrites, *Int. J. Biol. Macromol.*, 2020, **164**, 4245–4251.

15 R. Verma, S. Pathak, A. K. Srivastava, S. Prawer and S. Tomljenovic-Hanic, ZnO nanomaterials: Green synthesis, toxicity evaluation and new insights in biomedical applications, *J. Alloys Compd.*, 2021, **876**, 160175.

16 Q. Y. Tamboli, S. M. Patange, Y. K. Mohanta, R. Sharma and K. R. Zakde, Green synthesis of cobalt ferrite nanoparticles: an emerging material for environmental and biomedical applications, *J. Nanomater.*, 2023, **2023**(1), 9770212.

17 N. Jayaprakash, *et al.*, Green synthesis of Ag nanoparticles using Tamarind fruit extract for the antibacterial studies, *J. Photochem. Photobiol., B*, 2017, **169**, 178–185.

18 A. Gomathi, S. Rajarathinam and A. M. Sadiq, Phyto chemical screening of aqueous extract of Tamarind (Tamarindus indica L.) Shell, *Int. J. Basic, Appl. Innovative Res.*, 2017, **7**(11), 65–70.

19 S. Samejo, *et al.*, The green synthesis of magnesium oxide nanocomposite-based solid phase for the extraction of arsenic, cadmium, and lead from drinking water, *Anal. Methods*, 2023, **15**(31), 3863–3873.

20 L. Li, *et al.*, Chitosan/Al_2O_3-HA nanocomposite beads for efficient removal of estradiol and chrysoidin from aqueous solution, *Int. J. Biol. Macromol.*, 2020, **145**, 686–693.

21 M. Esmat, A. A. Farghali, M. H. Khedr and I. M. El-Sherbiny, Alginate-based nanocomposites for efficient removal of heavy metal ions, *Int. J. Biol. Macromol.*, 2017, **102**, 272–283.

22 R. Yadav and M. Agarwala, Phytochemical analysis of some medicinal plants, *J. Phytol.*, 2011, **3**(12), 10–14.

23 A. K. Tangra and G. S. Lotey, Synthesis and investigation of structural, optical, magnetic, and biocompatibility properties of nanoferrites $AFeO_2$, *Curr. Appl. Phys.*, 2021, **27**, 103–116.

24 A. Solunke, V. K. Barote, B. Sonawane, S. E. Shirsath, R. Kadam and V. S. Shinde, Sol-gel synthesis of Fe-rich cobalt ferrite nanoparticles and influence of pH concentration, *Mater. Today: Proc.*, 2023, **92**, 1225–1230.

25 O. Ozalp and M. Soylak, Ag modified ZnO nanoflowers for the dispersive micro-solid-phase extraction of lead (II) from food and water samples prior to its detection with high-resolution continuum source flame atomic absorption spectrometry, *Talanta*, 2023, **253**, 124082.

26 S. Perveen, *et al.*, Green Synthesis of Electroactive Magnesium Ferrite Nanoparticles for the Selective Determination of Mefenamic Acid in Blood, Pharmaceutical Products, and Wastewater, *Anal. Lett.*, 2024, 1–16.

27 X. Zhang, *et al.*, Potassium ferrite as heterogeneous photo-fenton catalyst for highly efficient dye degradation, *Catalysts*, 2020, **10**(3), 293.

28 O. A. El-Shamy, R. E. El-Azabawy and O. E. El-Azabawy, Synthesis and Characterization of Magnetite-Alginate Nanoparticles for Enhancement of Nickel and Cobalt Ion Adsorption from Wastewater, *J. Nanomater.*, 2019, **2019**(1), 6326012.

29 S. Hussain, *et al.*, Characterization and curve fittings of Mg+ 2 substituted R-type hexagonal ferrites, *Phys. B*, 2021, **605**, 412642.

30 A. Elahi, M. Ahmad, I. Ali and M. Rana, Preparation and properties of sol–gel synthesized Mg-substituted Ni2Y hexagonal ferrites, *Ceram. Int.*, 2013, **39**(2), 983–990.

31 A. Ohlan, K. Singh, A. Chandra and S. K. Dhawan, Microwave absorption behavior of core-shell structured poly (3, 4-ethylenedioxy thiophene)-barium ferrite nanocomposites, *AIP Adv.*, 2010, **2**(3), 927–933.

32 J. Han, Z. Zhou, R. Yin, D. Yang and J. Nie, Alginate–chitosan/hydroxyapatite polyelectrolyte complex porous scaffolds: Preparation and characterization, *Int. J. Biol. Macromol.*, 2010, **46**(2), 199–205.
33 T. Pongjanyakul, Alginate–magnesium aluminum silicate films: importance of alginate block structures, *Int. J. Pharm.*, 2009, **365**(1–2), 100–108.
34 Z. Dong, Q. Wang and Y. Du, Alginate/gelatin blend films and their properties for drug controlled release, *J. Membr. Sci.*, 2006, **280**(1–2), 37–44.
35 B. Sarmento, D. Ferreira, F. Veiga and A. Ribeiro, Characterization of insulin-loaded alginate nanoparticles produced by ionotropic pre-gelation through DSC and FTIR studies, *Carbohydr. Polym.*, 2006, **66**(1), 1–7.
36 T. Mimmo, C. Marzadori, D. Montecchio and C. Gessa, Characterisation of Ca–and Al–pectate gels by thermal analysis and FT-IR spectroscopy, *Carbohydr. Polym.*, 2005, **340**(16), 2510–2519.
37 S. Bajpai and S. J. R. Sharma, Investigation of swelling/degradation behaviour of alginate beads crosslinked with Ca2+ and Ba2+ ions, *React. Funct. Polym.*, 2004, **59**(2), 129–140.
38 S. E. McNeil, *Characterization of Nanoparticles Intended for Drug Delivery*. Springer, 2011.
39 I. P. S. Fernando, W. Lee, E. J. Han and G. Ahn, Alginate-based nanomaterials: Fabrication techniques, properties, and applications, *Chem. Eng. J.*, 2020, **391**, 123823.
40 K. Akhtar, *et al.*, Novel fluoride selective voltammetric sensing method by amino phenylboronic acid-zirconium oxide nanoparticles modified gold electrode, *Microchem. J.*, 2022, **174**, 107073.
41 K. Akhtar, *et al.*, Phytoextract based synthesis of TiO2. Al2O3 nanocomposites for efficient electrocatalytic detection of acetaminophen from environmental and pharmaceutical samples, *Ceram. Int.*, 2024, **50**(7), 11012–11021.
42 K. Akhtar, *et al.*, Biosynthesis of titanium oxide-aluminium oxide nanocomposites for electrocatalytic detection of 2, 4, 6-trichlorophenol, *Mater. Today Commun.*, 2024, **38**, 108137.
43 M. Safaei, H. Moradpoor, M. Salmani Mobarakeh and N. Fallahnia, Optimization of Antibacterial, Structures, and Thermal Properties of Alginate-ZrO2 Bionanocomposite by the Taguchi Method, *J. Nanotechnol.*, 2022, **2022**(1), 7406168.
44 C. M. De Ramos, *NMR Studies of Metal Ion Binding to Alginic Acid*, University of Cincinnati, 1995.
45 V. K. Gupta and I. Ali, Removal of lead and chromium from wastewater using bagasse fly ash—a sugar industry waste, *J. Colloid Interface Sci.*, 2004, **271**(2), 321–328.
46 O. Tünay and N. Kabdaşli, Hydroxide precipitation of complexed metals, *Water Research*, 1994, **28**(10), 2117–2124.
47 S. Yılmaz, B. Hazer and M. Tuzen, Extraction and preconcentration of lead (II) in various water and food samples by orbital shaker-assisted magnetic solid phase extraction method using a new magnetic poly linoleic acid-polystyrene-PDMS block copolymer, *Food Chem.*, 2024, **457**, 140114.
48 A. S. Amin, M. Y. Nassar and A. Gomaa, Utility of solid-phase extraction coupled with spectrophotometry for a novel green nano determination of copper (II) using 4-((furan-2-ylmethylene) amino)-5-methyl-4H-1, 2, 4-triazole-3-thiol, *Int. J. Environ. Anal. Chem.*, 2023, **103**(7), 1550–1571.
49 M. Soylak, H. E. H. Ahmed and M. Khan, Switchable hydrophilicity solvent based microextraction of mercury from water, fish and hair samples before its spectrophotometric detection, *Sustainable Chem. Pharm.*, 2023, **32**, 101006.
50 S. Perveen, *et al.*, Sodium nanoferrite-based solid phase extraction: a green method for the simultaneous determination of cadmium, copper, and lead, *J. Anal. At. Spectrom.*, 2024, **39**(11), 2884–2892.
51 S. G. Elci, A magnetic solid-phase extraction method using Fe3O4@ coPANI-PTH for microsample injection system-flame atomic absorption spectrometric determination of nickel and copper in soft drinks and spice samples, *Int. J. Environ. Anal. Chem.*, 2022, **102**(9), 2038–2052.
52 S. Ju, M. Liu and Y. Yang, Preconcentration and determination of cadmium, lead, and cobalt in Moringa oleifera (Moringaceae) using magnetic solid-phase extraction and flame atomic absorption spectrometry, *Anal. Lett.*, 2016, **49**(4), 511–522.
53 P. Liu, C.-N. Wang, X.-Y. Song and Y.-N. Wu, Dietary intake of lead and cadmium by children and adults–result calculated from dietary recall and available lead/cadmium level in food in comparison to result from food duplicate diet method, *Int. J. Hyg. Environ. Health*, 2010, **213**(6), 450–457.
54 Z. Atafar, *et al.*, Effect of fertilizer application on soil heavy metal concentration, *Environ. Monit. Assess.*, 2010, **160**, 83–89.
55 S. Giri and A. Singh, Human health risk assessment due to dietary intake of heavy metals through rice in the mining areas of Singhbhum Copper Belt, India, *Environ. Sci. Pollut. Res.*, 2017, **24**(17), 14945–14956.
56 H. E. H. Ahmed, A. M. A. Mohammed and M. Soylak, A magnetic solid phase extraction procedure for Pb (II) at trace levels on magnetic Luffa@ TiO2 in food and water samples, *Food Chem.*, 2023, **428**, 136794.
57 N. Baghban, E. Yilmaz and M. Soylak, Vortex assisted solid-phase extraction of lead (II) using orthorhombic nanosized Bi2WO6 as a sorbent, *J. Mol. Liq.*, 2018, **185**, 1–9.
58 M. B. Arain, H. E. H. Ahmed and M. Soylak, Dispersive solid phase microextraction (DSP-μE) by using nanodiamond@ Bi2MoO6 composite for the separation-preconcentration of Pb (II) in food and water samples, *Microchem. J.*, 2023, **195**, 109495.
59 H. E. H. Ahmed, O. Ozalp and M. Soylak, Magnetic solid phase extraction of lead (II) from food and water samples on magnetic MWCNTs/MgAl2O4/TiO2, *J. Food Compos. Anal.*, 2023, **118**, 105163.
60 M. B. Arain, H. E. H. Ahmed and M. Soylak, Functionalized nanodiamonds with NiCoFe layered double hydroxides used as a novel adsorbent in dispersive solid phase microextraction for Pb (II) determination in juice samples, *Microchem. J.*, 2024, **199**, 109922.
61 S. C. Tan and H. Lee, A hydrogel composite prepared from alginate, an amino-functionalized metal-organic

framework of type MIL-101 (Cr), and magnetite nanoparticles for magnetic solid-phase extraction and UHPLC-MS/MS analysis of polar chlorophenoxy acid herbicides, *Microchim. Acta*, 2019, **186**, 1–11.

62 M. Safari, R. Rezaee, R. D. C. Soltani and E. Asgari, Dual immobilization of magnetite nanoparticles and biosilica within alginate matrix for the adsorption of Cd (II) from aquatic phase, *Sci. Rep.*, 2022, **12**(1), 11473.

63 M. A. Serunting, R. Rusnadi, D. A. Setyorini and B. Ramadan, An effective cerium (III) ions removal method using sodium alginate-coated magnetite (Alg-Fe3O4) nanoparticles, *J. Water Supply: Res. Technol. – AQUA*, 2018, **67**(8), 754–765.

64 J. Shah and M. Jan, Eco-friendly alginate encapsulated magnetic graphene oxide beads for solid phase microextraction of endocrine disrupting compounds from water samples, *Ecotoxicol. Environ. Saf.*, 2020, **190**, 110099.